Directional memory arises from long-lived cytoskeletal asymmetries in polarized chemotactic cells

Harrison V. Prentice-Mott[a,b,c,1], Yasmine Meroz[c,1], Andreas Carlson[c], Michael A. Levine[a,b], Michael W. Davidson[d], Daniel Irimia[e], Guillaume T. Charras[f,g], L. Mahadevan[c,h,i,j,2], and Jagesh V. Shah[a,b,2]

[a]Department of Systems Biology, Harvard Medical School, Boston, MA 02115; [b]Renal Division, Brigham and Women's Hospital, Boston, MA 02115; [c]Paulson School of Engineering and Applied Sciences, Harvard University, Cambridge, MA 02138; [d]National High Magnetic Field Laboratory, Florida State University, Tallahassee, FL 32310; [e]Department of Surgery, Massachusetts General Hospital, Boston, MA 02129; [f]London Centre for Nanotechnology, University College London, London WC1H 0AH, United Kingdom; [g]Department of Cell and Developmental Biology, University College London, London WC1E 6BT, United Kingdom; [h]Department of Physics, Harvard University, Cambridge, MA 02138; [i]Organismic and Evolutionary Biology, Harvard University, Cambridge, MA 02138; and [j]Kavli Institute for Nanobio Science and Technology, Harvard University, Cambridge, MA 02138

Edited by Peter N. Devreotes, The Johns Hopkins University School of Medicine, Baltimore, MD, and approved November 30, 2015 (received for review July 7, 2015)

Chemotaxis, the directional migration of cells in a chemical gradient, is robust to fluctuations associated with low chemical concentrations and dynamically changing gradients as well as high saturating chemical concentrations. Although a number of reports have identified cellular behavior consistent with a directional memory that could account for behavior in these complex environments, the quantitative and molecular details of such a memory process remain unknown. Using microfluidics to confine cellular motion to a 1D channel and control chemoattractant exposure, we observed directional memory in chemotactic neutrophil-like cells. We modeled this directional memory as a long-lived intracellular asymmetry that decays slower than observed membrane phospholipid signaling. Measurements of intracellular dynamics revealed that moesin at the cell rear is a long-lived element that when inhibited, results in a reduction of memory. Inhibition of ROCK (Rho-associated protein kinase), downstream of RhoA (Ras homolog gene family, member A), stabilized moesin and directional memory while depolymerization of microtubules (MTs) disoriented moesin deposition and also reduced directional memory. Our study reveals that long-lived polarized cytoskeletal structures, specifically moesin, actomyosin, and MTs, provide a directional memory in neutrophil-like cells even as they respond on short time scales to external chemical cues.

confined cell migration | moesin | microtubules | chemotaxis | cell polarization

Directed cell motion underlies important functions in development, immunology, and resource foraging (1). The local cues for cellular orientation are chemical, either in the form of soluble gradients or substrate-bound moieties (2, 3), or physical, in the form of pressure, substrate adhesion, etc. (4, 5). In particular, chemical cues activate signaling at the cell surface and are integrated within the cell cytoplasm to give rise to a polarization in the direction of the local gradient. Although these processes have been the subject of detailed experimental study and theoretical and computational modeling, the mechanisms by which this orientation is achieved and maintained in the face of environmental noise remains incomplete.

Although migration might be thought of as being very sensitive to the variations in the external environment, instead, we see robust migration in a variety of fluctuating environments. These observations all point to the existence of a directional memory in chemotactic cells—a biochemical pathway that stores information about cellular orientation and prevents the loss of orientation in the face of fluctuations, transient loss of polarization, or saturation of the receptors. For example, recent work has demonstrated memory-based behavior in *Dictyostelium* amoebae under fluctuating waves of chemoattractant (6, 7), although the authors do not identify potential molecular elements that store this information.

Here, we use microchannel-based microfluidic devices to observe cell polarization and movement in confined mammalian neutrophil-like cells. Cells in this environment exhibit a strong bias to repolarize in the previous direction of motion after a period of depolarization. This memory is time-dependent and decays when the cell is unstimulated. To describe these results, we construct a minimal phenomenological model coupling membrane and cytoskeletal polarization lifetimes and show that this model provides a potential basis for this memory. We also show that the cytoskeletal ERM (Ezrin, Radixin, Moesin) family protein moesin has a long turnover time, in comparison with membrane phospholipid signaling, and that moesin inhibition results in a loss of memory. Depolymerization of microtubules (MTs) also disrupts memory, but by disrupting moesin localization, or reorienting the potential memory element. This membrane–cytoskeletal system acts to keep cells biased in their orientation based on previous signaling history potentially driving directed motility in noisy gradients.

Results

We adapted microfluidic devices that confine cell migration to a 1D geometry to allow independent and controlled exposure of chemoattractant to each side of the cell (Fig. S1*A*) (5, 8). Cells enter microchannels that connect two external reservoirs that

Significance

Cells orient their motility along chemical gradients using sensitive measurements of the external environment, a process termed chemotaxis. How cells sense, respond to, and remember varying environmental stimuli is only just beginning to be understood. Here, we identify a directional memory in chemotactic neutrophil-like cells. This memory allows cells to orient in low signal gradients and even uniform environments. This memory can be modeled by distinct time scales of chemical sensing and cytoskeletal dynamics, pointing to a general strategy of separating time scales for robust behavioral dynamics in cellular systems. Disrupting specific long-lived molecular assemblies erases directional memory. These studies reveal a novel directional memory resulting from distinct molecular time scales and contributing to chemotactic robustness in migrating cells.

Author contributions: H.V.P.-M., Y.M., L.M., and J.V.S. designed research; H.V.P.-M., Y.M., A.C., M.A.L., and L.M. performed research; H.V.P.-M., Y.M., M.W.D., D.I., and G.T.C. contributed new reagents/analytic tools; H.V.P.-M. and Y.M. analyzed data; and H.V.P.-M., Y.M., L.M., and J.V.S. wrote the paper.

The authors declare no conflict of interest.

This article is a PNAS Direct Submission.

[1]H.V.P.-M. and Y.M. contributed equally to this work.

[2]To whom correspondence may be addressed. Email: lm@seas.harvard.edu or jagesh_shah@hms.harvard.edu.

This article contains supporting information online at www.pnas.org/lookup/suppl/doi:10.1073/pnas.1513289113/-/DCSupplemental.

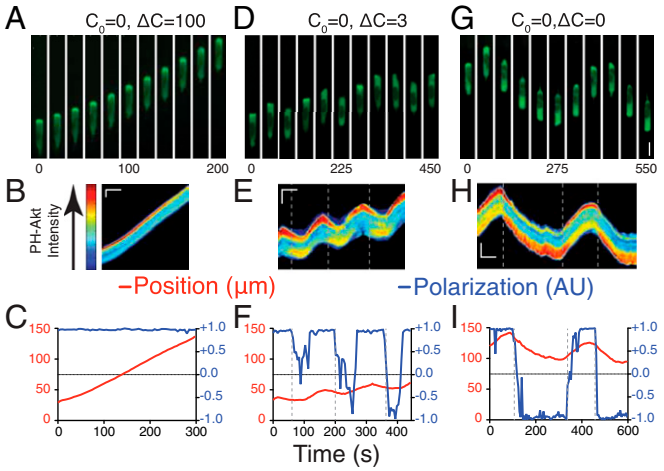

Fig. 1. Cellular response to static chemical environments. (*A*) Montages of cells expressing PH-Akt-GFP in the conditions $C_0 = 0$, $\Delta C = 100$. (*B*) Kymograph of cell shown in *A*, false-colored according to the color bar shown on the left. (*C*) Plots of cell centroid and PH-Akt polarization (*Experimental Procedures*) for corresponding montage and kymograph. (*D–F*) Montage (*D*), kymograph (*E*), and plots (*F*) for a cell in the condition $C_0 = 0$, $\Delta C = 3$. (*G–I*) Montage (*G*), kymograph (*H*), and plots (*I*) for a cell in the condition $C_0 = 0$, $\Delta C = 0$ (*C*). (Vertical scale for montages: *A*, *D*, and *G*, 10 μm; vertical scale bar for kymographs: *B*, *E*, and *H*, 15 μm; horizontal scale bar for kymographs: *B*, *E*, and *H*, 100 s.) Vertical dashed lines were added to both kymographs and time plots to represent the time at which the cell was determined to have depolarized.

maintain chemoattractant concentrations at each end. The microchannels are small enough (3 μm × 5 μm) that a single cell fills the cross-sectional area of the channel and acts as a barrier for fluid flow and diffusion, maintaining the concentration difference across the cell (Fig. S1*A*). Thus, the cell is exposed to differences between chemoattractant concentrations across it, and motion is restricted to 1D (up and down the channel). Moreover, the chemical exposure and cell geometry remain constant during cell motion, thus creating a stable fixed difference across the cell.

We subjected HL-60 (neutrophil-like) (9) cells to chemoattractant differences in formylated Met-Leu-Phe (fMLP). C_0 designates the concentration in the lower reservoir (i.e., [lower]), and ΔC designates the difference (i.e., [upper] − [lower]). For a 0–100 nM difference ($C_0 = 0$ nM and $\Delta C = 100$ nM), cells showed strong polarization toward the higher fMLP concentration, as seen by both morphology and the accumulation of PH-Akt-EGFP at the leading edge of the motile cell [marking PIP_3 lipids (10)] (Fig. 1 *A* and *B* and Movie S1). Quantitative analysis of cell polarization (11) and motility showed persistence in both measures (*SI Experimental Procedures*) for all cells measured (Fig. 1*C*). When cells were exposed to a smaller difference, cells were far less persistent ($C_0 = 0$ nM, $\Delta C = 3$ nM; Fig. 1 *D* and *E* and Movie S2). Quantitative analysis of cell polarization and motility showed fluctuations in both measures (Fig. 1*F*). The value 3 nM was chosen because it is well below the equilibrium dissociation constant (K_d) of the ligand fMLP for its receptor (10–15 nM) (12). Notably, cells that lose polarization exhibit a small motion opposite to their original direction of motion, a relaxation of its morphology, not a directed motion. Under saturating conditions ($C_0 = 50$ nM, $\Delta C = 50$ nM), where the background concentration of 50 nM is well above the receptor–ligand K_d (Fig. S1 *B* and *C* and Movie S3), we observed polarization persistence and directional changes similar to those seen for small differences (Fig. S1*D*).

Chemotactic cells can also undergo spontaneous polarization and motility in the absence of an external gradient, likely because of activation by extracellular matrix components such as fibronectin (13, 14). Observation of cells in 0–0 environments ($C_0 = 0$ nM, $\Delta C = 0$ nM) revealed cells with frequent switching of orientation and very few cells that maintained persistence across the entire channel (Fig. 1 *G–I* and Movie S4). When cells were placed in uniform environments of higher concentrations, we observed an increased level of persistent cells at 3 nM ($C_0 = 3$ nM, $\Delta C = 0$ nM; Fig. S1 *E–G* and Movie S5) that increased at 10 nM ($C_0 = 10$ nM, $\Delta C = 0$ nM; Fig. S1 *H–J* and Movie S6) and then dropped at 100 nM ($C_0 = 100$ nM, $\Delta C = 0$ nM; Fig. S1 *K–M* and Movie S7, with persistence quantified in Fig. S1*N*).

To quantify the polarization dynamics, we derived histograms of instantaneous cell polarization combining many cell trajectories (Fig. 2*A* and Fig. S2). All histograms show peaks near −1 and 1, reflecting the polarized state in both directions, and a small enrichment at 0 (the unpolarized state). The sign of the polarization was chosen such that the initial direction of polarization was positive. For persistently polarized cells, as observed in strong chemotactic differences (e.g., $C_0 = 0$ nM, $\Delta C = 100$ nM), cells exhibited a strong polarization bias toward +1 (Fig. S2*A*). At low chemoattractant differences (e.g., $C_0 = 0$ nM, $\Delta C = 3$ nM), we also observed a bias in polarization to the original direction of polarization with some fluctuation (Fig. S2*B*). This was also seen for differences on a large background concentration (e.g., $C_0 = 50$ nM, $\Delta C = 50$ nM; Fig. S2*C*). Histograms of cell polarization in uniform environments ($\Delta C = 0$ nM) revealed that cells in 3 and 10 nM also showed a nonzero bias (Fig. 2 *A* and *B* and Fig. S2 *E* and *F*). In the absence of chemoattractant (0 nM) and at 100 nM uniform concentration, the mean polarization moved closer to 0 (Fig. 2*A* and Fig. S2 *D* and *G*). The mean and skewness (a measure of asymmetry) of these distributions indicated a directional bias under both chemotactic differences and uniform conditions (Fig. 2*C*).

To understand this bias in uniform environments, we revisited the trajectories of single cells. A cell that repolarized in the original direction of polarization after a depolarization event was

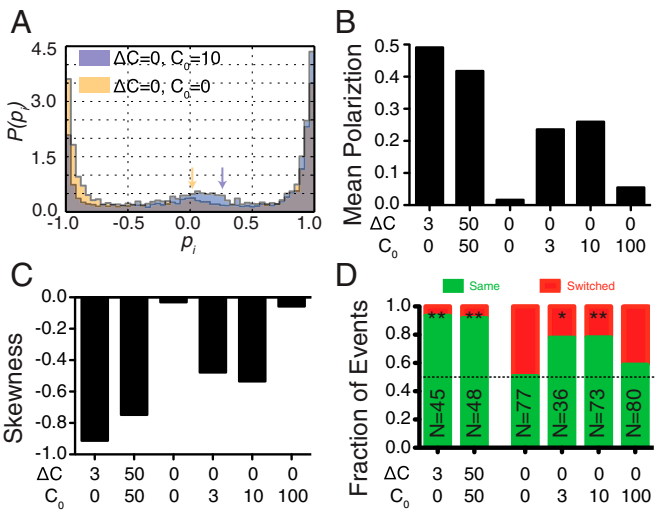

Fig. 2. Cells in uniform, nonzero concentrations exhibit a directional bias. (*A*) Histograms of instantaneous cell polarizations (PH-Akt) for cells in uniform concentrations of 0 nM (yellow) and 10 nM fMLP (blue). For the histograms shown all polarizations before the first depolarization of a cell were removed as described in the methods. Arrows designate the mean polarization. (*B*) Mean values for histograms of instantaneous polarizations. (*C*) Skewness of histograms of instantaneous polarizations (*SI Experimental Procedures*). (*D*) Statistics of repolarization direction. Green represents the percentage of events for which a cell repolarized in the same direction as before depolarization. Red represents the percentage of events for which a cell switched direction.

designated a "same" cell, whereas cells that repolarized in the opposite direction were designated as "switched." In environments with a chemical difference, cells exhibited a strong bias toward same (nonswitching) behavior (Fig. 2*D*). In some uniform environments, cells also exhibited strong nonswitching behavior, indicating a memory of the previous direction (e.g., 3 and 10 nM), whereas there was little to no bias in other uniform environments (e.g., 0 and 100 nM). Although the bias in the chemical difference environments might be expected, the bias seen in uniform environments, specifically 3 and 10 nM (~80%, $P < 0.004$; Fisher exact test), indicated that internal cellular factors can determine the direction of repolarization and not the external conditions.

To investigate the temporal dynamics of this memory, we used a dynamic environment to shift cells from a uniform environment with chemoattractant (C_0 = 10 nM, ΔC = 0 nM) to one with none (C_0 = 0 nM, ΔC = 0 nM) to promote depolarization at a specified time (Fig. 3*A*). Chemoattractant was then reintroduced after a time delay. The majority of cells depolarized under removal of the chemoattractant (69/77, 90%, Fig. S3*A*), exhibiting both chemical (PH-Akt-GFP) and morphological depolarization. After 2 min in the absence of chemoattractant, a uniform environment (C_0 = 10 nM, ΔC = 0 nM) was reestablished. Unpolarized cells reexposed to the uniform environment repolarized either in the same direction (Fig. 3*B* and Movie S8) to their previous motion or switched (Fig. 3*C* and Movie S9). Cells reexposed after 2 min of no chemoattractant exhibited a 90% bias toward the original direction (Fig. 3*D*). When extended out to 10 min of no chemoattractant, the bias dropped to 70%. During the 10-min depolarization time, many cells spontaneously polarized before the reintroduction of chemoattractant (29/65, 45%; Fig. S3*A*), and their directional bias toward the initial direction of polarization was ~80% (Fig. 3*D*, "Spontaneous"), indicating that the readdition of chemoattractant was not required to activate the polarization machinery but that the memory was still intact. Interestingly, a small number of cells (8/77, 10%) did not depolarize after removal of the chemokine, indicating some long-lived persistence in the absence of an external signal. We investigated the role of cell position in the channel given that some cells would experience differential temporal cues (front vs. back) if cells were closer to the channel ends. We found no correlation between the position in the channel and choice of polarization direction (Fig. S3*B*).

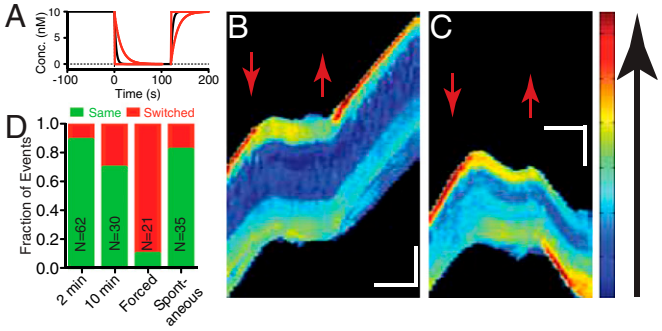

Fig. 3. Directional bias persists after removal of chemokine. (*A*) Calculated plot of concentration as a function of time in the microchannel (wash at t = 0 s; reintroduction at t = 120 s). Solid lines represent the decay attributable to diffusion for a distance of 50 μm (black), 100 μm (red, slow decay), and 10 μm (red, fast decay) from the end of the channel. (*B* and *C*) Kymographs representing a cell repolarizing in the same direction (*B*) and in the opposite direction (*C*). Red arrows mark the time when chemokine was removed (down) and reintroduced (up). (Vertical scale bar: 15 μm; horizontal scale bar: 100 s). (*D*) Repolarization direction statistics for cells exposed to the dynamic environment. Chemokine removal for 2 or 10 min. Repolarization by introducing chemokine only at the previous back of the cell ("Forced"). Spontaneous polarizations in the absence of chemokine are also shown.

We expected that a strong opposing chemoattractant difference would be capable of overcoming this memory. We modified the dynamic protocol to take cells from the no chemoattractant environment to a fixed difference (C_0 = 10 nM, ΔC = −10 nM) and found that for those cells initially polarized in the opposite direction to the final difference, 90% of the cells switched direction upon repolarization in the direction of the imposed difference (Fig. 3*D*, "Forced").

To quantify these observations in a minimal representation that accounts for the directional memory, we developed a phenomenological model for polarization dynamics as a function of the difference in concentration across the cell, ΔC, and the average concentration, $C_0 + \Delta C/2$. Our mathematical model represents the migrating cell as a composite of two interacting systems—a sensing unit embedded in the membrane and an actuating motor unit embedded in the cytoskeleton. The cytoskeleton can only indirectly sense the environment through the polarization state of the membrane; however, the cytoskeletal polarization biases membrane polarization much like the external environment does. We denote the membrane polarization by $p_m(t)$, as measured by PH-Akt-GFP activity, and we denote the cytoskeleton polarization by $p_c(t)$. Both of these variables can take values in the range of −1 to 1, where positive and negative values represent polarized states, and a vanishing value represents an unpolarized state. The dynamics of the system are modeled by a pair of Langevin-like equations for the membrane and cytoskeletal polarization, using a double-well potential that characterizes the two polarized states separated by an unpolarized state (Fig. 4*A*) and symmetry considerations:

$$dp_m/dt = -\alpha_m\, p_m(p_m-1)(p_m+1) + |\alpha_m|(\Delta n + p_c) + \eta_m, \quad \textbf{[1a]}$$

$$dp_c/dt = -\alpha_c\, p_c(p_c-1)(p_c+1) + |\alpha_c|p_m^* + \eta_m. \quad \textbf{[1b]}$$

The first term on each right-hand side arises from the derivative of the double-well potential, with three steady states corresponding to p_m, p_c = 0, +1, −1 (Fig. 4 *A*, *i* and *ii*). Here, α_m and $\alpha_c = \alpha_c(\alpha_m)$ are the stochastic gains for the membrane and cytoskeleton (which are functions of C via the fraction of bound receptors), so that for α_m, $\alpha_c < 0$, the unpolarized state is the only stable state, whereas for α_m, $\alpha_c > 0$, there are two stable states (p_m, p_c = +1; and p_m, p_c = −1) corresponding to polarization in the initial and opposite directions, respectively. A gradient in the chemokine concentration biases the preferred polarization and corresponds to the term Δn, the difference in the fraction of bound receptors, which breaks the symmetry of the potential landscape with a deeper well associated with the preferred polarization (Fig. 4 *A*, *iii*). The last term in each equation $\eta_m(t)$ is uncorrelated Gaussian noise. The second term in Eq. **1b** denotes the time-averaged membrane polarization $p_m^*(t) = \int_{-\infty}^{t} p_m(t)\,\Gamma(t-\tau)d\tau / \int_{-\infty}^{t} \Gamma(t-\tau)d\tau$, with $\Gamma(t) = Ae^{-t/\tau}$ denoting a memory kernel associated with the signaling cascade from the membrane to the cytoskeleton, with a characteristic time, τ. It has been observed that if the membrane depolarizes and repolarizes after a given time, it will repolarize in the direction dictated by the cytoskeletal polarization. This suggests a minimal coupling where the integration of the membrane polarization over time that biases p_c in the same direction, in turn biases p_m again (*SI Experimental Procedures, Model Description*). Eq. **1** together with a stochastically varying gain α_m (subject to receptor binding constraints; see *SI Experimental Procedures, Model Description*) form a complete set of equations for the dynamics of membrane and cytoskeleton polarization for some given initial conditions, with a single dimensionless parameter that controls the dynamical processes: $\tau\ \alpha_m$.

To gain some intuition about the model, we first look at the case $\tau = 0$, effectively decoupling p_m and p_c. Fig. 4*B* shows examples of simulated trajectories of $p_m(t)$. Because α_m is a function of the rate of binding events and noise, it responds to

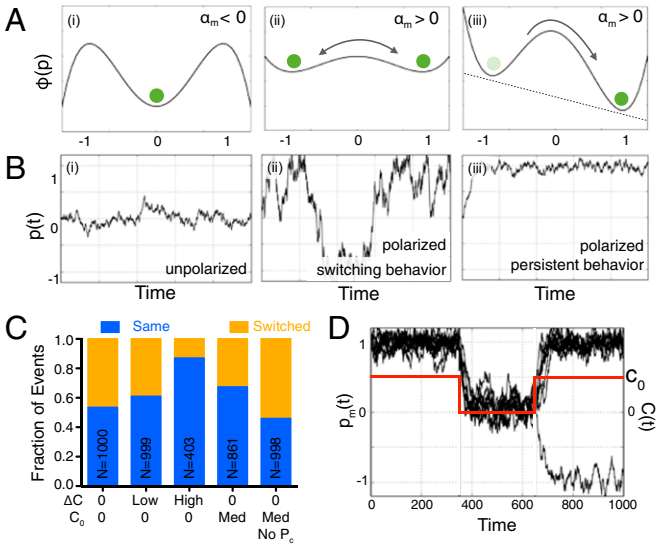

Fig. 4. Theoretical model of two-layer polarization reproduces directional bias. (*A*) Model effective potential wells, Φ(p), for a cell in a uniform low C_0 ($\alpha_m < 0$) (*i*), a uniform high C_0 ($\alpha_m > 0$) (*ii*), and $\Delta C > 0$ ($\alpha_m > 0$) (*iii*). (*B*) Simulated cells in the conditions in *A*: (*i*) cells fluctuate about the unpolarized state p = 0, (*ii*) cells tend to be in the polarized state p = ±1 and can switch direction, and (*iii*) cells remain persistently polarized. (*C*) Directional repolarization statistics for simulated cells for different cases of C_0 and ΔC, including no coupling to p_c. (*D*) Simulations of the dynamic experiments exhibiting memory, where $C(t) > 0$ (plotted in red as a function of time), then $C(t) = 0$ (and cells depolarize), and then $C(t) > 0$ again, whereupon the vast majority of simulated cells repolarize in the original direction.

external conditions by switching between polarization directions and between polarized and unpolarized states. For $\alpha_m < 0$, the effective potential landscape exhibits a single well corresponding to the unpolarized state (Fig. 4 *B*, *i*). For $\alpha_m > 0$ and $\Delta n = 0$, the landscape switches to a symmetric double well corresponding to two polarized orientations (Fig. 4 *B*, *ii*). If Δn now increases above 0, the potential becomes asymmetric favoring the polarization in the direction of Δn (Fig. 4 *B*, *iii*). Next, we introduce memory with nonzero τ that couples p_m and p_c, and we carry out simulations following the direction in which a cell repolarizes following a depolarization event. In the absence of any chemokine, simulated cells exhibited no bias in the repolarization direction (Fig. 4*C*), whereas the introduction of even a small concentration difference resulted in a measurable bias, which increased with the magnitude of Δn. Fig. 4*D* shows that we qualitatively reproduce experimental behavior. In addition, cells in a uniform C_0 also exhibited a directional bias (absent for $\tau = 0$). These simulations also recovered distributions of instantaneous polarization (Fig. S4). Simulations of dynamic removal and reintroduction of chemokine (as in Fig. 3*A*) showed a strong bias to repolarizing in the same direction as the original polarization (Fig. 4*D*). Increasing the time for reintroduction of chemokine decreased the fidelity of the directional memory. Increasing τ, which simulates longer cytoskeletal time scales, resulted in a longer-lived directional memory (Fig. S4*E*).

Our model also naturally allows us to explain seemingly paradoxical behaviors observed in other chemotactic systems. Indeed, in *Dictyostelium*, Nakajima et al. (9) showed that the speed of waves of chemoattractant affect the migration behavior, dubbing this the "wave-paradox"; for fast waves, no migration is observed; for slow waves, cells move toward the incoming wave but reverse their direction as the wave passes the cell; whereas for intermediate wave velocities, cells migrate toward the incoming wave throughout the wave cycle, resulting in forward cell migration in a negative chemotactic gradient. We now turn to describe this phenomenon using our two-layered mathematical model. We define two time scales in these experiments: $\tau_{\Delta n}$, the time scale of the positive gradient (half the time the wave needs to cross the cell); and τ_{pc}, the time scale of the memory kernel. As the wave comes in, it imposes a positive gradient $\Delta n > 0$ while $p_c = 0$; therefore, the total bias is positive, and p_m increases with time to its maximum value +1. The temporal integration of p_m biases p_c, which therefore increases. After the wave passes the cell, the external gradient switches sign (i.e., $\Delta n \rightarrow -\Delta n$). For slow waves (i.e., $\tau_{\Delta n} > \tau_{pc}$), upon switching of the gradient, p_c will have already reached its maximum value, and therefore the total bias ($-\Delta n + p_c$) effectively diminishes with time and eventually switches signs (i.e., p_m also switches signs) (Fig. S4*F*). For intermediate waves (i.e., $\tau_{\Delta n} \sim \tau_{pc}$), upon switching of the gradient, p_c has not reached its maximum value yet and is still increasing, effectively canceling out the negative bias of the gradient $-\Delta n$ (i.e., p_m does not switch signs) (Fig. S4*G*). As with previous work in *Dictyostelium* (6, 7), which uses the more complex LEGI+M (local excitation–global inhibition plus memory) model, our model explains both directional memory and the wave paradox. We point out that the main differences lie in the reduced complexity of our model. In particular, our holistic model led us to three equations that characterize the dynamics of the observable chemical polarization of the membrane p_m, the mechanical polarization of the cytoskeleton p_c, as well as the gain associated with chemokine binding α, permitting the identification of putative cellular components corresponding to these variables with six parameters, which depend on the environment: K_d, the dissociation constant; k_+, the association rate; η_m and η_α, the magnitude of noise; n_{on}^{min}, the minimal bounds for α; and, lastly, τ, the extent of the memory kernel.

Two molecular assemblies that might serve as repositories of this long-lived asymmetry driving directional memory are the actomyosin network and the ERM–actin–membrane structures that localize to the rear of a polarized cell (15, 16). Both structures have been previously shown to exhibit turnover times that are long compared with PH-Akt dynamics in other cell types (17, 18). We introduced mApple-fusions to myosin light chain (MLC) and moesin into PH-Akt-GFP–expressing HL-60 cells. Polarization decay of mApple-MLC, after chemoattractant removal, was similar to that of PH-Akt-GFP (Fig. 5 *A* and *B*, Fig. S5*A*, and Movie S10). Unlike MLC, the mApple-moesin remained polarized longer than PH-Akt-GFP, after chemoattractant removal, indicating longer-lived asymmetry within the cell (Fig. 5 *C* and *D*, Fig. S5*B*, and Movie S11). Whereas the decay rate was only slightly faster, the most obvious difference was the delay in moesin depolarization, which resulted in a rapid increase in the cumulative difference between moesin and PH-Akt polarization compared with MLC vs. PH-Akt (Fig. S5*C*).

Moesin is a member of the ERM family of proteins that acts to connect the plasma membrane (via PIP_2) to the cortical actin cytoskeleton (19–21). A critical threonine residue is present in the C terminus of each of the ERM family members that regulates the interaction with f-actin, and the N-terminal FERM (Band4.1, Ezrin, Radixin, Moesin) domain regulates an interaction with MTs (22). A quinolone-based compound (NSC668394) was previously developed to bind this threonine and prevent its phosphorylation, disrupting f-actin binding (23). Addition of NSC668394 at 50 μM to the dynamic protocol (during the no chemoattractant phase) resulted in a reduction of directional memory from 90% to 60% (Fig. 5*E*). Blebbistatin, a myosin II inhibitor (50 μM) also decreased directional memory (24) (Fig. 5*E*).

The ROCK (Rho-associated protein kinase) kinase is a downstream effector of Rho-GTP, an integrator of the back domain (25), and ROCK's inhibition [via Y27632, 20 μM (26)] did not decrease directional memory (Fig. 5*E*). A significant number of cells under ROCK inhibition and chemoattractant removal continued to move along the channel (Fig. S5*D*). The combination of ROCK and

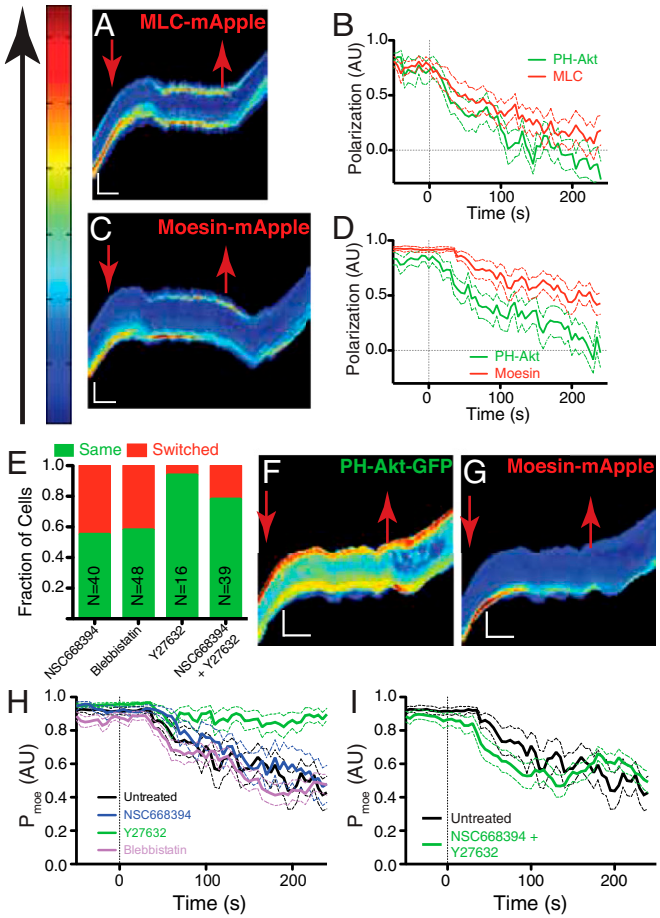

Fig. 5. Identification of long-lived cytoskeletal polarization. (*A*) Representative kymograph MLC-mApple in a cell exposed to the dynamic environment described in Fig. 3*A*. (*B*) Average relaxation curves for MLC-mApple and PH-Akt-GFP polarization. (*C* and *D*) Kymograph and average relaxation curves for moesin-mApple. (*E*) Directional repolarization statistics for cells exposed to the dynamic environment (Fig. 3) with drugs introduced upon chemokine removal and washed out upon chemokine reintroduction. (*F* and *G*) Kymographs of PH-Akt-GFP (*F*) and moesin-mApple (*G*) for a cell dynamically exposed to the ROCK inhibitor Y27632. Note the prolonged polarization of moesin in *G* compared with *C*. (*H* and *I*) Average relaxation curves of moesin-mApple polarization for single drugs (*H*) and their combination (*I*). Decay plots represents the average value (solid) and SD (dashed). Red arrows mark the time when chemokine was removed (down) and reintroduced (up). (Vertical scale bar: 15 μm; horizontal scale bar: 100 s.)

moesin inhibition preserved memory. To understand the interrelationship between these components, we investigated the decay of moesin under each of these drugs. Interestingly, ROCK inhibition stabilized moesin at the back of the depolarized cell independently of PH-Akt (Fig. 5 *F* and *G* and Movie S12). All other treatments had no effect on the decay of moesin (Fig. 5*H*, Fig. S5 *E* and *F*, and Movie S13). The addition of the moesin inhibitor to ROCK inhibition partially restored moesin decay dynamics (Fig. 5*I*).

Treatment of chemotactic cells with colcemid (10 μM), a MT-depolymerizing compound during the no chemoattractant phase, resulted in the mislocalization of moesin and PH-Akt (Fig. S6 *A* and *B* and Movie S14), effectively accelerating the decay of moesin polarization and reducing directional memory (Fig. 6 *A* and *B*). Addition of the ROCK inhibitor to colcemid resulted in a stabilization of the mislocalized moesin at both the front and back of the cell (Fig. S6 *C* and *D* and Movie S15) and thus a reduction of memory (Fig. 6 *A* and *B*). This stabilization resulted in a dramatic increase in cells that did not repolarize after the reintroduction of chemoattractant and drug washout (Fig. S6*E*).

Discussion

Observations of chemotactic neutrophil-like cells in a variety of chemical differences and uniform environments revealed a bias in repolarization directions toward that of previous cellular orientations. A model based on long-lived asymmetric cellular elements that persist after cells have depolarized and that influence orientation upon repolarization was able to recapitulate many aspects of this memory.

Observations of internal dynamics revealed that moesin is a strong candidate for this memory because moesin had the requisite long-lived behavior and moesin's inhibition reduced directional memory. Although moesin exhibited the long polarization time scale indicative of a directional memory (exhibiting faster decay and delay in depolarization), inhibition via the small quinolone molecule did not change moesin dynamics but did interrupt memory. The action of NSC668394 is to block T558 phosphorylation on moesin and decouple moesin from f-actin (23). This decoupling may accelerate the depolarization of the actual memory element. Alternatively, the phosphosite itself may act to bias repolarization (27).

Blebbistatin also reduced memory, thereby implicating myosin as a potential memory element. This result was surprising given that MLC polarization decay did not exhibit the appropriate time scale to account for the observed directional memory (as shown in Fig. 5*B* and Fig. S5*C*). However, it is possible that myosin heavy chain localization remains polarized on a longer time scale than does the polarization of MLC (the regulatory light chain). Recent work identifying a serine-rich motif in myosin heavy chain II-B regulating cell polarization highlights a potential candidate (28). Under ROCK inhibition, moesin and likely myosin were stabilized, thereby promoting memory and indicating a link between RhoA (Ras homolog gene family, member A) activity and moesin turnover (29). However, the combination of ROCK and moesin inhibition restored moesin decay dynamics but still exhibited some memory supporting a role for actomyosin.

MT disruption also reduces directional memory but by mislocalizing moesin rather than accelerating its decay from the cell membrane. Loss of MTs in neutrophils has been previously associated with loss of polarity and reduced directional migration (30). Here we propose that the role of MTs acts to focus biochemical activities to maintain proteins such as moesin (and myosin) at the back domain, as has been observed in other cell types (31). One candidate for this regulation would be RhoA that has been linked to MTs through the MT-bound RhoGEF, GEF-H1 (32).

Together these data support a model of cellular orientation that depends on both external environmental cues and internal membrane lipid composition that polarize long-lived cytoskeletal markers that act as a form of directional memory. Models which

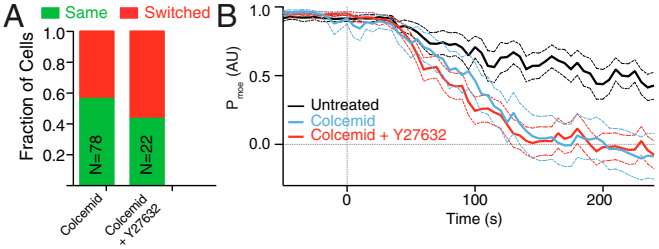

Fig. 6. MT disruption alters moesin polarization and disrupts memory. (*A*) Directional repolarization statistics for cells exposed to colcemid alone or colcemid and Y27632. (*B*) Average relaxation curves of moesin-mApple for untreated cells, cells exposed to colcemid and cells exposed to both colcemid and Y27632. Solid lines represent the average value across the population, dashed lines represent one SD.

focus only on the early chemotactic response associated with membrane polarization, e.g., LEGI would be unaffected by cytoskeletal perturbations. Our observations under perturbations of moesin and myosin show that this is not the case, thus requiring that we couple the dynamics of cytoskeletal and membrane polarizations.

Further dynamical tests in confined geometries and 2D chemotactic fields should help refine the layered model and account for additional time and length scales associated with complex spatiotemporal signaling [e.g., small GTPases (15)] within the cell. For example, the model predicts that when the new external cue is aligned with the internal memory it may establish polarization more rapidly than when an external cue is oriented in opposition to the internal memory. Further, kinetic measurements would begin to dissect interprocess time scales and explain behaviors such as U-turns originally described by Zigmond et al. (33) that occur at slow changes in the external environment but disappear in rapidly changing gradients (34) and maintain polarity in the face of reversed chemoattractant gradients (35). More generally, our study shows how the temporal separation of membrane and cytoskeletal polarizations allows a cell to sense and respond to a fluctuating environment robustly.

Experimental Procedures

Cell Culture and Stable Line Production. HL-60 cell lines were generated and maintained as previously described (5), with details in the *SI Experimental Procedures*. Dual expression cell lines were generated via lentiviral infection of cells stably expressing PH-Akt-GFP with either MLC-mApple or hsMoesin-mApple.

Microfluidic Device Operation. Operation of the microfluidic devices was carried out as previously described (5, 8) with details available in the *SI Experimental Procedures*. To expose cells to dynamic changes in concentration, cells were loaded and allowed to enter the microchannels in a uniform concentration of 10 nM fMLP by clamping off the 0 nM reservoir. The chemokine was then washed away by clamping off the 10 nM inlet and releasing the 0 nM reservoir. Chemokine was reintroduced by clamping the 0 nM inlet and releasing the 10 nM inlet. Inhibitors were added to the 0 nM reservoir (*SI Experimental Procedures*).

Image Acquisition and Analysis. The cell polarization was determined using a clustering method similar to that described by Ku et al. (11) with details in the *SI Experimental Procedures*. To determine cell persistence, cells that maintained a polarized morphology and a polarization parameter >0.8 (the threshold) throughout the entire length of the channel, or during the entire period of imaging, were determined to be persistent. Transient fluctuations of the polarization parameter below the threshold for a single frame were still determined to be persistent. In the case that the polarization parameter remained below the threshold for two or more frames, the cell was determined to have depolarized. Repolarization events were identified if the polarization parameter increased above the threshold and a morphological polarization was established.

Note Added in Proof. During the preparation of this manuscript, a report by Maiuri et al. (36) demonstrated that retrograde flow during migration increases the asymmetry of cell-polarity cues, thus maintaining cell polarization (i.e., persistence). It is possible that this effect on polarization is related to the coupling we suggest between membrane and cytoskeletal polarization, drawing a parallel between directional memory and persistence.

ACKNOWLEDGMENTS. The authors thank the members of the J.V.S. and L.M. laboratories and Tim Mitchison for valuable discussions. Microfabrication work was supported by BioMEMS Resource Center Grant P41 EB002503. This work was supported by Biological and Biotechnological Sciences Research Council Grant BB/F021402 (to G.T.C.), Brigham and Women's Renal Division funds (to J.V.S.), National Science Foundation Grant BMMB 15-36616 (to J.V.S. and L.M.), and a MacArthur Fellowship (to L.M.). Y.M. is an Awardee of the Weizmann Institute of Science–National Postdoctoral Award Program for Advancing Women in Science.

1. Swaney KF, Huang C-H, Devreotes PN (2010) Eukaryotic chemotaxis: A network of signaling pathways controls motility, directional sensing, and polarity. *Annu Rev Biophys* 39:265–289.
2. Zigmond SH (1974) Mechanisms of sensing chemical gradients by polymorphonuclear leukocytes. *Nature* 249(456):450–452.
3. Brandley BK, Schnaar RL (1989) Tumor cell haptotaxis on covalently immobilized linear and exponential gradients of a cell adhesion peptide. *Dev Biol* 135(1): 74–86.
4. Lo C-M, Wang H-B, Dembo M, Wang YL (2000) Cell movement is guided by the rigidity of the substrate. *Biophys J* 79(1):144–152.
5. Prentice-Mott HV, et al. (2013) Biased migration of confined neutrophil-like cells in asymmetric hydraulic environments. *Proc Natl Acad Sci USA* 110(52):21006–21011.
6. Skoge M, et al. (2014) Cellular memory in eukaryotic chemotaxis. *Proc Natl Acad Sci USA* 111(40):14448–14453.
7. Nakajima A, Ishihara S, Imoto D, Sawai S (2014) Rectified directional sensing in long-range cell migration. *Nat Commun* 5:5367.
8. Irimia D, Charras G, Agrawal N, Mitchison T, Toner M (2007) Polar stimulation and constrained cell migration in microfluidic channels. *Lab Chip* 7(12):1783–1790.
9. Millius A, Weiner OD (2009) Chemotaxis in neutrophil-like HL-60 cells. *Methods Mol Biol* 571:167–177.
10. Meili R, et al. (1999) Chemoattractant-mediated transient activation and membrane localization of Akt/PKB is required for efficient chemotaxis to cAMP in Dictyostelium. *EMBO J* 18(8):2092–2105.
11. Ku C-J, Wang Y, Weiner OD, Altschuler SJ, Wu LF (2012) Network crosstalk dynamically changes during neutrophil polarization. *Cell* 149(5):1073–1083.
12. Williams LT, Snyderman R, Pike MC, Lefkowitz RJ (1977) Specific receptor sites for chemotactic peptides on human polymorphonuclear leukocytes. *Proc Natl Acad Sci USA* 74(3):1204–1208.
13. Li L, Nørrelykke SF, Cox EC (2008) Persistent cell motion in the absence of external signals: A search strategy for eukaryotic cells. *PLoS One* 3(5):e2093.
14. Bosgraaf L, Van Haastert PJM (2009) Navigation of chemotactic cells by parallel signaling to pseudopod persistence and orientation. *PLoS One* 4(8):e6842.
15. Xu J, et al. (2003) Divergent signals and cytoskeletal assemblies regulate self-organizing polarity in neutrophils. *Cell* 114(2):201–214.
16. Seveau S, Keller H, Maxfield FR, Piller F, Halbwachs-Mecarelli L (2000) Neutrophil polarity and locomotion are associated with surface redistribution of leukosialin (CD43), an antiadhesive membrane molecule. *Blood* 95(8):2462–2470.
17. Wang Y, et al. (2013) Identifying network motifs that buffer front-to-back signaling in polarized neutrophils. *Cell Rep* 3(5):1607–1616.
18. Fritzsche M, Thorogate R, Charras G (2014) Quantitative analysis of ezrin turnover dynamics in the actin cortex. *Biophys J* 106(2):343–353.
19. Neisch AL, Fehon RG (2011) Ezrin, Radixin and Moesin: Key regulators of membrane-cortex interactions and signaling. *Curr Opin Cell Biol* 23(4):377–382.
20. Bretscher A, Edwards K, Fehon RG (2002) ERM proteins and merlin: Integrators at the cell cortex. *Nat Rev Mol Cell Biol* 3(8):586–599.
21. Kunda P, Pelling AE, Liu T, Baum B (2008) Moesin controls cortical rigidity, cell rounding, and spindle morphogenesis during mitosis. *Curr Biol* 18(2):91–101.
22. Solinet S, et al. (2013) The actin-binding ERM protein Moesin binds to and stabilizes microtubules at the cell cortex. *J Cell Biol* 202(2):251–260.
23. Bulut G, et al. (2012) Small molecule inhibitors of ezrin inhibit the invasive phenotype of osteosarcoma cells. *Oncogene* 31(3):269–281.
24. Straight AF, et al. (2003) Dissecting temporal and spatial control of cytokinesis with a myosin II Inhibitor. *Science* 299(5613):1743–1747.
25. Wong K, Pertz O, Hahn K, Bourne H (2006) Neutrophil polarization: Spatiotemporal dynamics of RhoA activity support a self-organizing mechanism. *Proc Natl Acad Sci USA* 103(10):3639–3644.
26. Uehata M, et al. (1997) Calcium sensitization of smooth muscle mediated by a Rho-associated protein kinase in hypertension. *Nature* 389(6654):990–994.
27. Liu X, et al. (2015) Moesin and myosin phosphatase confine neutrophil orientation in a chemotactic gradient. *J Exp Med* 212(2):267–280.
28. Juanes-Garcia A, et al. (2015) A regulatory motif in nonmuscle myosin II-B regulates its role in migratory front-back polarity. *J Cell Biol* 209(1):23–32.
29. Ivetic A, Ridley AJ (2004) Ezrin/radixin/moesin proteins and Rho GTPase signalling in leucocytes. *Immunology* 112(2):165–176.
30. Xu J, Wang F, Van Keymeulen A, Rentel M, Bourne HR (2005) Neutrophil microtubules suppress polarity and enhance directional migration. *Proc Natl Acad Sci USA* 102(19): 6884–6889.
31. Zhang J, Guo WH, Wang YL (2014) Microtubules stabilize cell polarity by localizing rear signals. *Proc Natl Acad Sci USA*.
32. Kwan KM, Kirschner MW (2005) A microtubule-binding Rho-GEF controls cell morphology during convergent extension of Xenopus laevis. *Development* 132(20):4599–4610.
33. Zigmond SH, Levitsky HI, Kreel BJ (1981) Cell polarity: An examination of its behavioral expression and its consequences for polymorphonuclear leukocyte chemotaxis. *J Cell Biol* 89(3):585–592.
34. Irimia D, et al. (2006) Microfluidic system for measuring neutrophil migratory responses to fast switches of chemical gradients. *Lab Chip* 6(2):191–198.
35. Robertson AL, et al. (2014) A zebrafish compound screen reveals modulation of neutrophil reverse migration as an anti-inflammatory mechanism. *Sci Transl Med* 6:225ra229–225ra229.
36. Maiuri P, et al. (2015) Actin flows mediate a universal coupling between cell speed and cell persistence. *Cell* 161(2):374–386.
37. Chung SH, Kennedy RA (1991) Forward-backward non-linear filtering technique for extracting small biological signals from noise. *J Neurosci Methods* 40(1):71–86.